JOURNAL OF MECHANICAL ENGINEERING AND SCIENCES (JMES)
ISSN: 2289-4659 e-ISSN: 2231-8380
VOL. 16, ISSUE 3, 9043 – 9055
DOI: https://doi.org/10.15282/jmes.16.3.2022.07.0716

ORIGINAL ARTICLE

Tribological behavior of steel-steel pair: Influence of roughness and cutting parameters

H. Bouhabila[1, 2*], A. Bouchoucha[1], A. Merabet[1], R. Benzerga[3] and C. Le Paven[3]

[1] Mechanical laboratory, Mechanical Engineering Department, Faculty of Science of Technology, University Frères Mentouri, Constantine, 25000, Algeria.
[2] Mechanical Engineering Department, Faculty of Science and Applied Science, University of Oum El-Bouaghi, 4001, Algeria.
Phone: 21332 47 54 51; Fax.; 21332 47 54 51
[3] Science and Engineering Materials Department, IUT of Saint Brieuc, University of Rennes 1, 22000, France.

ABSTRACT – Roughness characterizes the quality of the machined surfaces, mainly determined by the geometric tolerances and induced by the different factors involved in the cutting process. The aim of this paper is to study the influence of cutting parameters (cutting speed (V_c), feed rate (f), tool nose radius (R_c) and cutting depth (a_p)), on the cylinder surface roughness, in order to value the friction coefficient (μ) and the wear rate (W) of the contact surfaces of steel-steel pair: 42CrMo4-20MnCr5. Full factorial design (DOE) of 9 tests is used, to develop theoretical model of the roughness of machined metal parts on turning. Hence, the influence of the cylinder roughness on the friction and wear behavior of the steel-steel pair contact is studied, using a pin-cylinder tribometer. The results revealed that the friction coefficient and wear rate, increases progressively by varying the surface roughness (cutting parameters). The processing and observations of the results were recorded using a profilometer, an optical microscope, a scanning electron microscopy (SEM) followed by an analysis in energy dispersive spectroscopy (EDS). However, the surface of the pin is plowed, cracked and plastically deformed, thus inducing more loss of material by adhesion and oxidation of the formed particles on the cylinder, which bring about a material transfer and formation of a metal oxide layer.

ARTICLE HISTORY
Received: 09th Dec. 2021
Revised: 12th Apr. 2022
Accepted: 15th July 2022

KEYWORDS
Surface roughness
Cutting parameters
DOE
Tribology
Friction
Wear
Steel-steel pair

INTRODUCTION

Industrial automation aims to obtain better production quality which is directly related to the implementation method and the roughness of the surface [1]. The latter is one of the most relevant mechanical characteristics in metal cutting as it represents the final control stage of the production cycle. It is necessary to choose the most suitable metal in terms of nuance and characteristics and to theoretically model the influence of cutting speed, feed rate and tool nose radius in the cutting process in order to choose the most suitable ones that would yield the most optimal surface quality [2, 3]. Aouisi et. al. explored the impact of cutting parameters such as cutting speed, feed rate, and cutting duration on surface roughness (Ra) on machinability, the processing conditions are turning of hardened hot work steel (AISI H11) with CBN tools using both response surface methodology (RSM) and ANOVA to developed mathematical models [4]. Using Taguchi approach, Sahua and Choudhuryb studied the effects of cutting parameters such as cutting speed, feed rate, and depth of cut on surface roughness. They examined the surface morphology and used the data to predict tool wear [5]. Taguchi's experimental design method was implemented by Menghani et al. to examine the effects of the impact of velocity, angle, coating material and the discharge rate of erodent on erosion wear rate of different coatings [6]. Wagh et al. have studied structural and mechanical properties such as hardness and wear resistance. The effects of laser hardening process on Ck45 steel cylindrical sample was investigated by using Taguchi's optimization technique [7].

The dry and permanent contact between the two parts, of a somehow good quality, engenders a severe wear which needs to be studied. Many researchers have differently studied wear influenced by different parameters. Archard's approach defined the wear rate of a couple of materials depending on material intrinsic factors and as relating to contact conditions such as applied load, the sliding speed and the presence or the absence of lubricant [8]. Kerridge and Lancaster demonstrated the possibility of transferring the material from the hard disk to the pin, increasing the hardness of the contact surface of the pin, reducing therefore, the wear rate [9]. Ayel presented two actions in this respect: the formation of minute chips through shearing and the plastic deformation which causes material displacement [10]. Bhushan concluded that the variation of friction depends on interfacial conditions such as roughness, type of material, system rigidity, lubrication, normal load, geometry, relative motion and sliding velocity [11]. The choice of the steel for the parts submitted to wear is found to be affected by the surface hardness of the component [12]. Wear, which may be affected by mating partners, normal load, sliding speed, temperature, finish surface, atmosphere, lubrication or corrosion, was investigated by Khanafi et al. [13]. Viafara and Sinatora showed that the difference in hardness of the mating parts has a significant impact on the contact surface life [14]. Panin and al. showed that sliding wear is driven by processes of abrasion, adhesion and delamination. This process may be caused by fragmentation of the softer material resulting in the

*CORRESPONDING AUTHOR | H. Bouhabila | ✉ hamoudi_bouhabila@yahoo.fr

formation of debris [15]. The small debris particles created by plastic deformation are trapped in the contact zone that is influenced by the third body particles, affecting the variation in the friction coefficient and this has been approved by Diomidis and Mischler [16]. According to Wang and al., the wear particles can oxidize and become hard abrading oxides due to the energy dissipated in the contact, and this is liable to increase the wear rate [17].

Thus, the current study directly links the impact of cutting parameters and roughness on tribological behaviour (friction coefficient and wear rate), which is dependent on the nature and shape of the cylinder-pin contact. Using ANOVA and response surface methods (RSM), mathematical model has been developed. Then, the two nuances: 42CrMo4-20MnCr5 chosen in the tribological behaviour investigation of dry or lubricated contact steel-steel pair material are used in camshaft and rocker arm in thermal engines. The contact studied depends on the result of the roughness Ra obtained from machining of the same cylinder, with a motionless pin on tribometer elaborated in advance [18]. The friction coefficient (dry or lubricated) is determined by means of a data acquisition. However, the value of wear rate (weight loss of the pin), has been obtained after weighing successive to each test.

EXPERIMENT

The objective is to investigate the tribological contact (dry or lubricated) in a system while using two mechanical parts in steel, of different shades, in permanent contact (such as: camshaft and rocker arm in thermal engines) in order to evaluate the friction coefficient and the wear rate in terms of the surface condition. The aim is to implement different roughness's in the cylinder surface (via varying the cutting parameters: cutting speed (Vc), feed rate (f), tool nose radius (Rc), divided into several tracks, in constant contact each with a pin, to study the tribological behaviour in friction and wear.

Machining and Measuring

The cylindrical disk with diameter ϕ = 40 mm, length L = 134 mm, of 42CrMo4 grade is fixed on a parallel turn (power P = 4.9 kW) using a mixed assembly (see Figure 1(a)). Nine (9) tracks were machined, with different selected cutting parameters: cutting speed (Vc) ranging from 800 to 1600 $m.min^{-1}$, feed rate (f) ranging from 0.15 to 0.25 $mm.rev^{-1}$ and tool nose radius (Rc) varying from 0.5 to 1.5 mm, are presented in Table 1. The operation carried out is the turning in finishing pass (ap) constant of 0.5 mm. The second cylinder of 20MnCr5 grade, is implemented so as to make the different pieces (9 pins for 9 tracks), according to the method of experimental plans DOE see thereafter.

A couple of material, different shades (hard-tender) were chosen; The 42CrMo4 for the cylinder is a pre-processed steel used for loaded transmission parts: camshaft, cylinders, gears and crowns; the 20MnCr5 for the pin is a more or less hard and resistant processing steel, often used for: the rocker finger, the bushings, the chain sprockets and the pins [19, 20, 21].

Table 1. Assignment of the levels to the factors

Level	Cutting speed ($m.min^{-1}$)	Feed rate ($mm.rev^{-1}$)	Tool nose radius (mm)
1	800	0.15	0.5
2	1600	0.25	1.5

The mechanical properties and the chemical composition of the different steels used are shown in (Table (2) and (3)).

Table 2. Chemical composition

Element of the tribological couple	Designation	Chemical composition				
		%C	% Mn	% Si	% Cr	% Mo
Pin	20MnCr5	0.12	1.07	0.24	1.0	0.014
	Standards value	0.17 - 0.22	1.1 - 1.4	< 0.4	1.0 - 1.3	---
Cylinder	42CrMo4	0.41	0.86	0.22	1.11	0.22
	Standards value	0.42	0.75	0.25	1.10	0.22

Table 3. Mechanical characteristics

Standard	Elastic Limit≥ [N/mm^2]	Tensile strength [N/mm^2]	Strain ratio %	Stiction at Break %	Resilience [J]	Hardness [HV] 20 Kg Load
20MnCr5	240	450-600	24	45	27	240-270
42CrMo4	650	900-1100	12	50	35	340-355

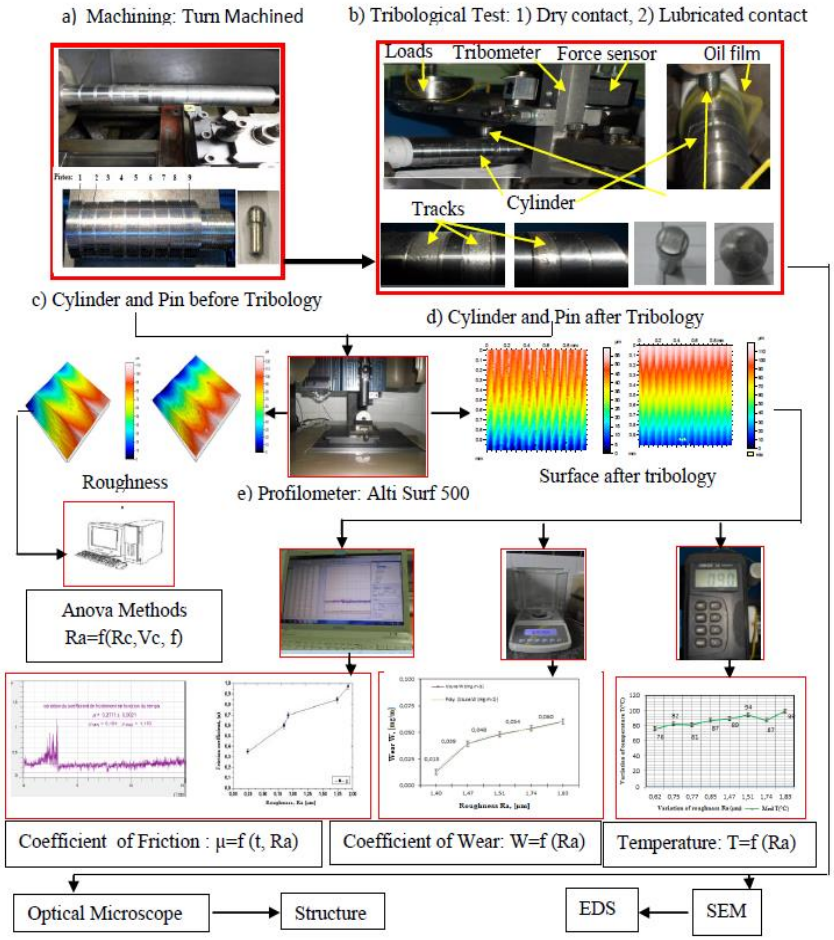

Figure 1. Schematic diagram of the experimental process

For the purpose of profile study and for the determining of the real roughness value, we used a profilometer (Alti Serf 500) fit with 3D image processing software and a 2D roughness profile (Figure 1(e)), the implemented scanning is perpendicular to the generator striations [21]. Two arithmetic roughness measuring (Ra) have been implemented, the first is the outcome of the finishing straight turning operation of each track according to the different cutting parameters used (Figure1(e) and 2), and the second after tribological test (Figure 9 and 10).

An example of the results of the roughness Ra before tribological test is presented in Figure 2.

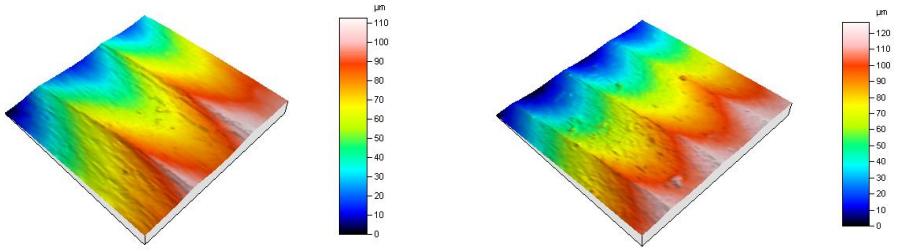

(a) (b)

Figure 2. Example of roughness Ra results before tribological test, for: Rc=1.5 [mm], f= 0.15 [mm.rev^{-1}], N=20[N] (a) Vc = 800 [m.min^{-1}], Ra_1 = 0.815 [μm] and (b) Vc = 1600 [m.min^{-1}], Ra_2 = 0.636 [μm]

Experimental Design and Results

The response surface methodology (RSM) is the procedure for determining the relationship between the independent process parameters with the desired response and exploring the effect of these parameters on responses, including six steps. The first (1) is define the independent input variables and the desired responses with the design constants, adopt an experimental design plan, (2) calculate the statistical analysis of variance (ANOVA) for the independent input variables in order to find which parameter significantly affects the desired response, (3) perform regression analysis with the quadratic model of RSM, (4) determine the situation of the quadratic model of RSM andfinally, (5) Optimize and conduct confirmation experiment, (6) Evaluation of roughness deviations [22, 23, 24]. The target of this experimental experience plans (DOE), is to highlight the impact of the three (3) selected parameters: the cutting speed (Vc), the tool nose radius (Rc) and the feed rate (f), upon the roughness (Ra) for material 42CrMo4.

Ra Matrix Program (MP)

For the selected experimental conditions, three (3) input impact factors (Vc, Rc, f), having two (2) levels and a single response which the objective function, represented by the Ra, consists of eight trials (2^3 trials) [23, 25], are presented in Table 4.

Table 4. Matrix program and measured values of the objective function (Ra)

Test Number	Impact factors						Function Objective
	Codified Values			Physical values			
	V_c	R_c	f	V_c [m.min^{-1}]	R_c [mm]	f [mm.rev^{-1}]	R_a [µm]42CrMo4
1	-1	-1	-1	800	0.5	0.15	2.414
2	+1	-1	-1	1600	0.5	0.15	1.566
3	-1	+1	-1	800	1.5	0.15	0.815
4	+1	+1	-1	1600	1.5	0.15	0.636
5	-1	-1	+1	800	0.5	0.25	3.694
6	+1	-1	+1	1600	0.5	0.25	2.39
7	-1	+1	+1	800	1.5	0.25	1.717
8	+1	+1	+1	1600	1.5	0.25	1.064

ANOVA for the Surface Roughness, Ra

The results of variance analysis (ANOVA) for surface roughness are shown in Table 5. The analysis is carried out for a significance level $\alpha = 0.5$, (i.e. for a confidence level of 95%). In this table, the degrees of freedom (DF), sum of squares (SC sq.), mean square (MS), F-values and probabilities (P-value), in addition to the contribution (Cont. %) of each factor, are also shown. The ANOVA results show that the tool nose radius (Rc) is the most important factor influencing surface finish Ra (see Table 5). It makes up 58.73%. The feed rate (f) is the second component that influences Ra. It makes up 20.36%. Cutting speed (Vc) accounts for 15.37%. On the arithmetic mean Ra, the interaction tool nose radius / feed rate has no statistical relevance [4, 5].

Table 5. Analysis of variance for Ra

Source	DF	SC $_{sq.}$	MS	F-Value	Prob > F	Cont.%	Effect	Coef Mod
Model	6	7.239	1.207	29791.776	0.0044			1.787
Vc	1	1.113	1.113	27482.272	0.0038	15.37	-0.746	-0.373
Rc	1	4.252	4.252	104976.00	0.0020	58.73	-1.458	-0.729
f	1	1.474	1.474	36396.160	0.0033	20.36	0.859	0.429
Vc x Rc	1	0.218	0.218	5377.777	0.0087	3.01	0.330	0.165
Vc x f	1	0.108	0.108	2669.444	0.0123	1.49	-0.233	-0.116
Rc x f	1	0.075	0.075	1849.000	0.0148	1.03	-0.194	-0.097
Vc x Rc x f			0.4E-4			0.56E-3	-0.005	-0.373
Residual	1	0.4E-4						
Total	7	7.23944				100		

Results of the Parameters Impact

Figure 3 shows the impact result caused by the influencing factors and their interactions on the objective function Ra, in the form of a PARETO histogram [26, 27]. The results show that the roughness is mainly influenced by the tool nose

radius (Rc), and at a lesser grade by the feed rate (f) and the cutting speed (Vc). If the tool nose radius varies from 0.5 to 1.5 mm, the Ra decreases by 1.46 µm. On the other hand, if the feed rate varies from 0.15 to 0.25 mm/rev, the Ra increases by 0.86 µm. The main influencing factors and their interactions are listed in Table 5, in decreasing order with respect to the impact caused by these factors.

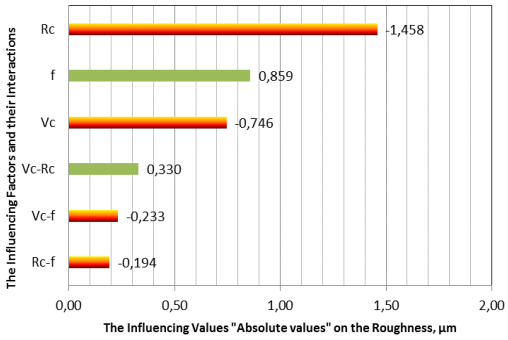

Figure 3. Influence of the cutting parameters (Rc, f, Vc) on the roughness

Roughness Modeling: A Developed Model

In the case of a turning operation, on a parallel turn, the shape of the machined surface depends on the geometrical features of the cutting edge of the tool and the feed rate for a constant pass [19, 20, 21]. As a result, aim to find out the influence factor of each of the cutting parameters on the machined surface quality using the experimental design method (DOE). From the histograms of PARETO in figure 4 and the coefficients of influence factors (2^3), its necessary to write the variation characteristics Eq. (3) of Ra according to the operating parameters of section (Vc, Rc, f). In the current study, the relationship between the cutting conditions and the machinability aspect is given:

$$Y = \Phi\left(Vc,\ f,\ Rc\right) \tag{1}$$

Where, Y is the desired machinability aspect and (Φ) is the response function. The approximation of Y is proposed by using a non-linear (quadratic) mathematical model, which is suitable for studying the interaction effects of process parameters on machinability characteristics. In the present work, the RMS based second order mathematical model is given by [4]:

$$Y = a_0 + \sum_{i=1}^{k} b_i X_i + \sum_{i,j}^{k} b_{ij} X_i X_j + \sum_{i=1}^{k} b_{ii} X_i^{\ 2} \tag{2}$$

Where, b_0 is the free term of the regression equation, the coefficients (b_1, b_2, ..., b_k *and* b_{11}, b_{22}, ..., b_{kk}) are the linear and the quadratic terms respectively; while (b_{12}, b_{13}, ..., $b_{1\text{-}k}$) are the interacting terms. The experimental plan is developed to assess the influence of cutting speed (Vc), feed rate (f) and tool nose radius (Rc) on the surface roughness. Two levels are defined for each cutting variable as given in Table 1. The variable levels are chosen within the intervals recommended by cutting tool manufacturer. Three cutting variables at two levels led to a total of 8 tests.

Final equations of the influence factors obtained from the calculation, for 42CrMo4, we have:

$$Ra = 1.787 - 0.373 \times Vc - 0.729 \times Rc + 0.429 \times f + 0.165 \times Vc \times Rc - 0.116 \times Vc \times f - 0.097 \times Rc \times f \tag{3}$$

For the roughness, the average value obtained in Table 5, is 1.787 µm, the coefficients associated with each influence factor are equal to half of the amplitudes [16], presented in the histogram (see Figure 3).

Finally, the values (Vc, Rc and f) entered in the estimation equation are values calculated by the following expression:

$$X_{icod} = \frac{X_{iphys} - X_{i0phys}}{I_{iphys}} \tag{4}$$

With X_{i0phys} : central level of the influence factor (i);

I_{iphys} : variation interval of the influence factor (i) and i = 1, 2.

The predicted values of response factors Ra from regression equations, Eq. (3) corresponding to different combinations of machining parameters are reported in Table 8. Moreover, they are compared with the corresponding experimental values illustrated in Figure 5.

B-3D Roughness Analysis

The variations of the roughness depending on the significant or non-significant influence factors can be observed in Figure 4; which shows that the tool nose radius (Rc), the feed rate (f) and the cutting speed (Vc) and their interaction have

significant impacts on the roughness. For low speeds, the effect of the tool nose radius (Rc) on the roughness is greater than the one for high speeds (see Figure 4), but for the feed rate (f) it has the opposite impact, the roughness decreases by decreasing the feed rate (f) for high cutting speeds (Vc), and increases by increasing the feed rate for low cutting speeds.

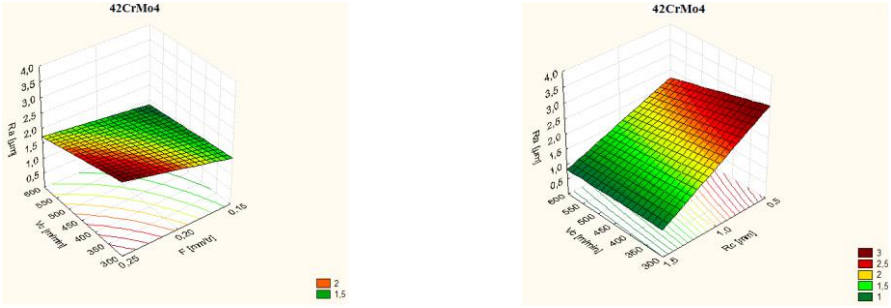

(a) (b)

Figure 4. Variation of roughness (Ra) with respect to: (a) Vc, Rc and (b) Vc, f

Optimization of Cutting Conditions

The optimal manufacturing conditions for machining with the constraints of cutting parametric range is that corresponding to lower values of Ra during the turning. The constraints used during the optimization process are summarized in Table 6, whereas the optimal solutions are reported in Table 7 in order of decreasing desirability level. Table 7 shows the (RSM) optimization results for surface roughness. The optimum cutting parameters obtained in Table 7 for cutting speed of 1600 $m.min^{-1}$, feed rate of 0.15 $mm.rev^{-1}$ and tool nose radius of 1.5 mm. The optimized Ra are 0.63375 to 0.64349 µm. A higher correlation coefficient value of R^2 of 0.999 which shows the correctness of the mathematical model used [4, 6, 7].

Table 6. Constraints for optimization of cutting conditions

Condition	Goal	Lower Limit	Upper Limit
Cutting speed, Vc	Is in range	800	1600
Tool nose radius, Rc	Is in range	0.5	1.5
Feed rate, f	Is in range	0.15	0.25
Rugosite, Ra	Minimize	0.636	3.694

Table 7. Optimization results

Solutions N°	Vc, m/min	Rc, mm	f, mm/rev	Ra, µm	Desirability
1	1600	1.50	0.15	0.63375	1
2	1600	1.50	0.15	0.63591	1
3	1600	1.50	0.15	0.63596	1
4	1600	1.50	0.15	0.63586	1
5	1600	1.50	0.15	0.63923	0.99894
6	1600	1.50	0.15	0.64071	0.99846
7	1600	1.50	0.15	0.64189	0.99808
8	1600	1.50	0.15	0.64349	0.99755
R-Squared	0.99999	**Pred R-Squared**	0.99964		
Adj R-Squared	0.99996	**Adeq Precision**	514.4516		

Evaluation of Roughness Deviations

The experimental values of Ra are compared to the values estimated by the empirical model for the 8 trials in order to evaluate the robustness of the empirical model (Table 8 and Figure 5). It is found that there is a significant coherence between the experimental and the values estimated by the Eq. (3). A relative variance of 0.0008 percent to 0.003 percent are shown in Table 8. As a result, the empirical model can be determined to be useful. The differences calculated as a percentage between the experimental roughness and that estimated by the model are shown in Table 8, the maximum error estimate does not reach the 5% value, showing thus its significance, which shows the correctness of the mathematical model used.

Table 8. Roughness comparison (measurements-estimates)

N° Test	Ra $_{exp}$, µm	Ra $_{mod}$, µm	Error %
1	2.390	2.388	0.0008
2	1.717	1.715	0.0012
3	1.064	1.066	0.0019
4	3.694	3.696	0.0005
5	1.566	1.568	0.0013
6	0.815	0.817	0.0025
7	2.414	2.412	0.0008
8	0.636	0.634	0.0031

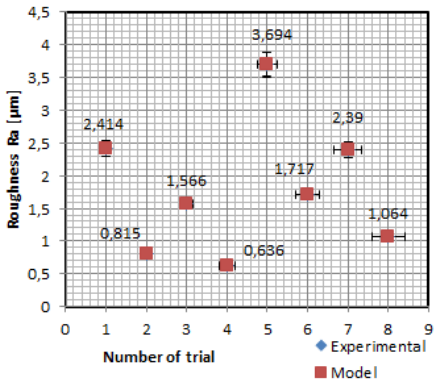

Figure 5. Roughness comparison (measurements against estimates)

Tribological Test

The set (previously machined cylinder-pin (Figure 1(c)) is mounted on a device (tribometer realized) to perform the tribological test. The tribological study of the steel-steel pair [18], shades (42CrMo4 and 20MnCr5), was carried out on this device made in the laboratory (pin-cylinder tribometer) fit with an acquisition device and software (CASSY Lab) to record the coefficients of friction, thus the forces generated (tangential and normal force) see Figure 6 and 7. The tests were conducted in an atmospheric environment. The dry tests made it possible to obtain values of the friction coefficient (μ_{dry}) from 0.2 to 2 (Figure 11(a) and 7(a)). For such a reason, 10W40 industrial oil was used to lubricate the dynamic contact [28]. Under these conditions, the $\mu_{lubricated}$ decreases from 0.2 to 0.5. (see Figure 11(b) and 7(b)).

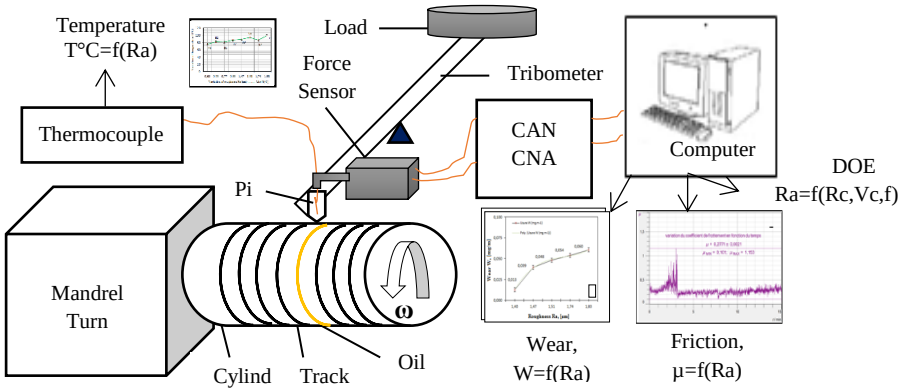

Figure 6. Schematic diagram for the experimental setup

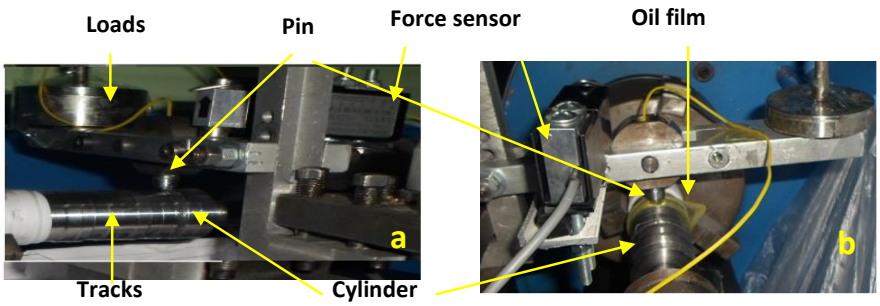

Figure 7. Tribometer mounted on a parallel turn machine, (a) Dry contact, (b) Lubricated contact

RESULTS AND DISCUSSION

Figure 8 shows the real state of the parts (cylinder and pin) after tribological dry or lubricated test, we notice worn out tracks of the cylinder. The track (a) corresponds to the pin (1) in dry contact, roughness of 0.98µm (see Figure 10(a)), its shape is wider and deeper, presence of debris on the surface (Figure 8(a)), which corresponds to removal of the material from the worn out pin; then for the track (b) which corresponds to the pin (2) in lubricated contact, a roughness of 1.47µm, less wide and laminated surface have extensive smooth slabs almost polished, almost brown colour, absence of debris that have been evacuated by the oil used (Figure 8(b)).

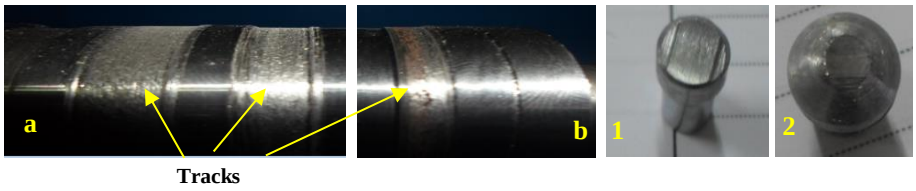

Figure 8. Cylinder and pins track after tribology: (a) and (1) Dry contact, (b) and (2) Lubricated contact

The results obtained by the profilometer, show that the value of the Ra decreases from 2.41 to 0.98 µm (see Figure 9(a) and 10(a)), during dry contact for a roughness quality therefore a reduction of 1.43 µm; on the other hand for a better and polished quality, it decreases from 1.57 to 1.47 µm as can be shown in Figure 9(b) and 10(b); during the lubricated contact therefore a decrease of 0.1 µm. This explains during dry contact, a disappearance of roughness peaks and a considerable increase in the wear rate of the part in permanent contact (cylinder), for Ra = 1.4 to1.83 µm, corresponds W = 0.013 to 0.06 mg/m, as can be noticed on Figure 15(a). In lubricated contact, positive effect of the oil which reduces the wear rate and guarantees a good surface (Figure 15(b)); for Ra = 0.62 to 0.85 µm, corresponds W = 0.0008 to 0.0028 mg/m [18, 29]. After tribology, a reduction in the maximum value of (Ra) due to the disappearance of the peaks under the effect from higher shears stress at the level of the asperities. This phenomenon yields a considerable wear of the cylinder surface. For a load N = 20N and a cutting speed Vc = 800 m.min^{-1}, the variation of the friction coefficient (µ) with respect to time (Figure 11) shows that the friction coefficient remains almost constant throughout the unfolding of the test, while, its value varies according to the variation of the initial roughness of the used cylinder μ_{dry} are 0.2 to 2 and μ_{lub} are 0.2 to 0.5, for Ra = 0.64 to 3.69 µm (see Table 4).

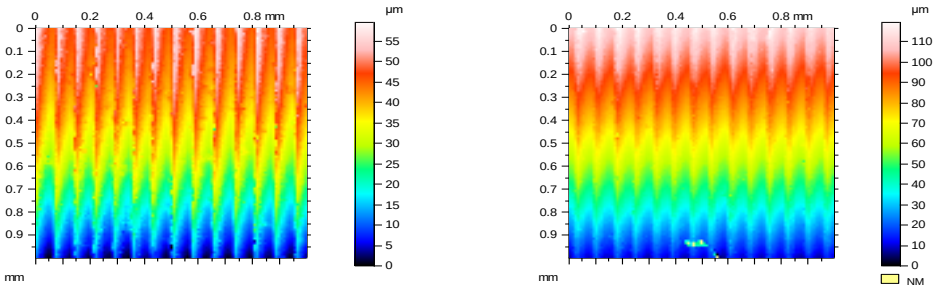

(a) (b)

Figure 9. Example of roughness, (Ra) for 42CrMo4, after machining: (a) Vc = 800 [m.min^{-1}], Ra_1 = 2.41 [µm] and (b) Vc = 1600 [m.min^{-1}], Ra_2 = 1.57 [µm]

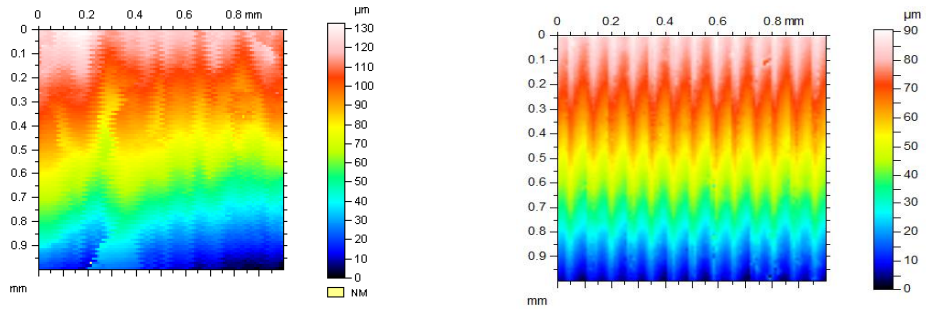

(a) (b)

Figure 10. Example of roughness, (Ra) for 42CrMo4, after tribological test, Vc = 800 [m.min^{-1}]
(a) Dry contact, Ra_3 = 0.98 [µm] and (b) Lubricated contact, Ra_4 = 1.47 [µm]

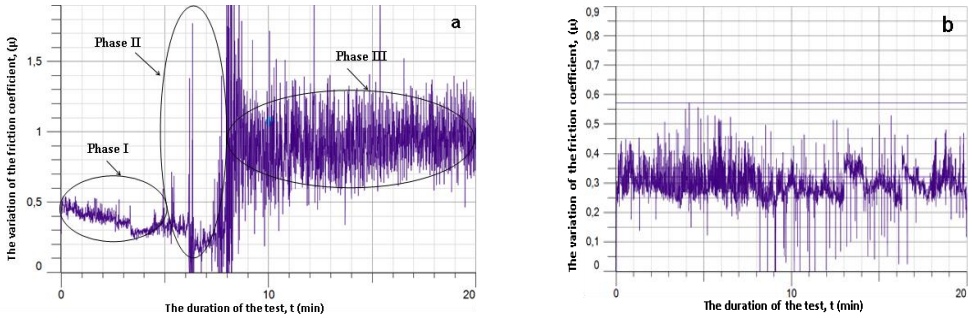

Figure 11. Variation of the friction coefficient with respect the duration, N=20[N],Vc=800[m.min^{-1}],
(a) dry contact: Ra_6 = 1.74 [µm], μ_{dry} = 0.7; (b) lubricated contact: Ra_7 = 1.5 [µm], μ_{lub}= 0.3

During the unfolding of the dry contact test (see Figure 11(a)), the obtained results show the presence of three distinct phases:

A-First Phase: this is a break-in phase, a first contact of the asperities, which lasts about 1 to 5 minutes and during which the coefficient of friction varies between 0.5 to 0.2, according to the roughness of the selected track.

B- Second Phase: it is a distorted phase (transient), which lasts approximately 2 to 3 minutes, where the asperities of the antagonists become entangled thus increasing the contact and the adhesion, μ_{dry} = 0.2 to 2. The hardest cylinder peaks (see the structure of the cylinder, shade 42CrMo4 (Figure 12(a)), presence of perlite more than ferrite the which increases the hardness of the material) that the counter face thrust into the surface of the metal of the pin, plowing the latter along the contact and tearing off the material which form weather-strips at the edges of the surface as can be shown in (Figure 16 (c) and (d)) and supported by [30].

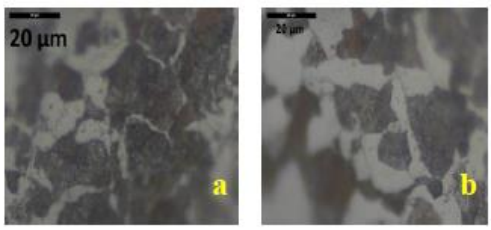

Figure 12. Images of the material structure with optical microscope at 20 [µm] and 50 [µm]:
(a, b) nuance 42CrMo4 (c, d) nuance 20MnCr5

The plastic deformation results in an average temperature rise at the interface between 70°C and 100°C (Figure 13(a)); the latter was noticed, using a thermocouple placed (2mm) off the contact [18, 31]. This temperature rise affects the mechanical properties of the surfaces [13, 29], such as the elastic limit and shear stress of the softest material (see the structure of the pin of 20MnCr5 nuance, (Figure 12(b)), presence of ferrite more than perlite the which weakens the structure), thus reducing the friction (Figure 14(b)) and thus increasing the wear rate of the pin (Figure 15(b)).

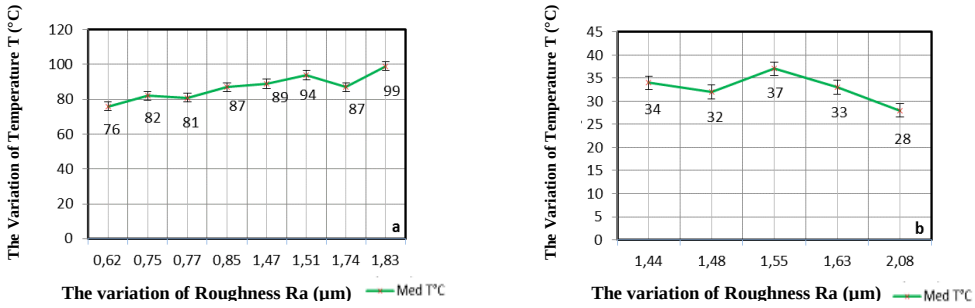

(a) (b)

Figure 13. Variation of the medium temperature T [°C] with respect to roughness Ra [µm]: (a) Dry contact and (b) Lubricated contact

C-Last Phase: it represents the steady state part; during this long phase (rest of the test duration of 15 to 20 minutes) the equilibrium state is established by the stability of the operating conditions at the interface [31]. In this zone the friction coefficient decreases is in the range of 0.6 to 1.3 as can be shown in Figure 11(a), depending on the chosen track, while the temperature varies according to the test is decreased at the end of 100°C to 25°C (see Figure (13)) [31].

Figure 11(b), shows the evolution of the friction coefficient (µ) in lubricated contact, the lubrication facilitates the sliding [28], as can be show in Figure 16 (a, d) and decreases the effect of the shear stresses generated during the test carried out, then disappearance of the zone disturbed. During this test, the friction coefficient decreases is in the range of 0.3 to 0.6 depending on the chosen track, while the temperature remains almost constant according to the test is decreased from 37°C to 28 °C (Figure 13(b)). Therefore, the cracks disappear (Figure 16 (a, d) and (µ) decreases [29].

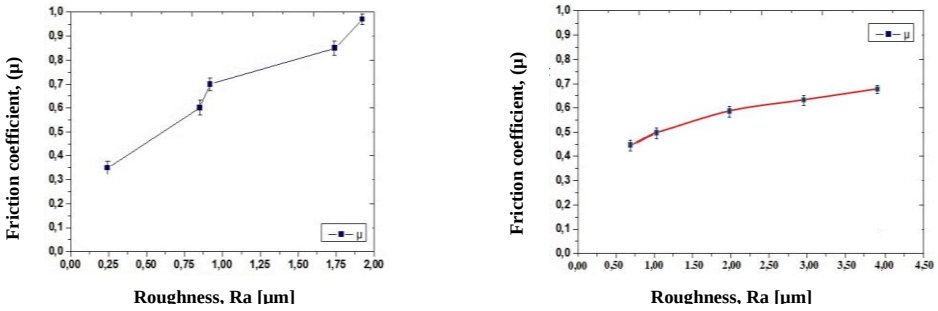

(a) (b)

Figure 14. Variation of the friction coefficient (µ) with respect to roughness (Ra) (a) Dry contact and (b) Lubricated contact

Figure 14 shows the evolution of the friction coefficient (µ) with respect to the Ra, for both tested cases (with as well as without lubrication), indeed (µ) increases when the Ra increases, in dry contact for Ra = 0.25 to 1.9 µm corresponds µ= 0.35 to 0.95, in lubricant contact for Ra = 0.5 to 3.94 µm corresponds µ = 0.4 to 0.7. The roughness of the cylinder has a directly influence on the friction coefficient [8].

Figure 15 shows the evolution of the wear rate (W) with respect to the Ra, for both tested cases does indeed (W) increase from 0.0125 to 0.06 mg.m^{-1} when Ra increases from 1.40 to 1.83 µm. The roughness values reflect the better quality of the cylinder surface prior to the test (Figure 9(b)), which is of higher hardness 340 HV as can be shown in Figure 12(a), these peaks will act positively and progressively by varying their value, plowing the surface of the pin (see Figure 16(c) and (d)) of lower hardness 240 HV (Figure 12(b)) [30], and increase the (W), this result has been asserted by Lepesant and Bouchoucha [32, 33].

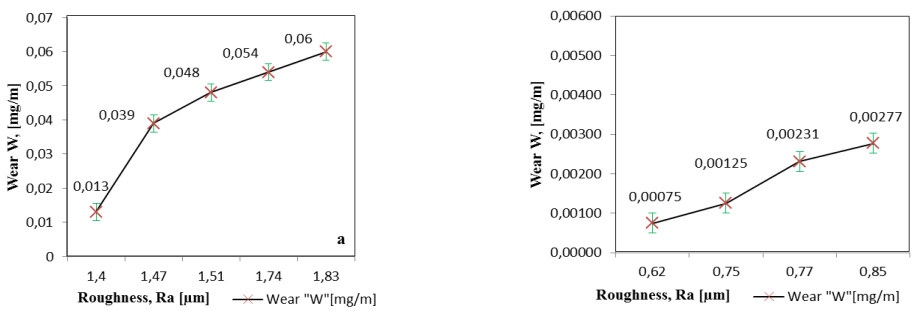

(a) (b)

Figure 15. Variation of wear (W) with respect to roughness (Ra): (a) Dry contact, (b) Lubricated contact

The present result shows that the cylinder roughness has a particular influence on the wear rate as Archard has shown [8]. Hence, the presence and engendering of cracks along the pin contact area has been observed in Figure 16(c), given the severe operating conditions, and the cyclic stresses exerted on the surface [31]. These cracks give rise to fatigue wear which generates active debris of medium size at the interface, these debris accumulate and thrust into the pin by tearing off the metal (abrasive wear) (see Figure 16(d)) [16, 33]. As can be noticed an action of the oxides (brown color on the track of the cylinder in Figure 8(b)) due to the increase of the temperature during the plastic deformation (T_{max} = 100 °C), as confirmed in Figure 16 (c, d) spectra of the pin tested in both conditions; dry and lubricated.

Moreover, there was a transfer of material from the pin to the tracks in contact with the cylinder during the test (Figure 16(b) and 17(a)), as confirmed by Kerridge and Mouadji [9, 31]. The asperities or hard particles can be likened to micro-tools. They cause displacement of material by shearing and micro-chip formation or by plastic deformation, confirmed by Ayel and Khanafi-Benghalem [10, 13].

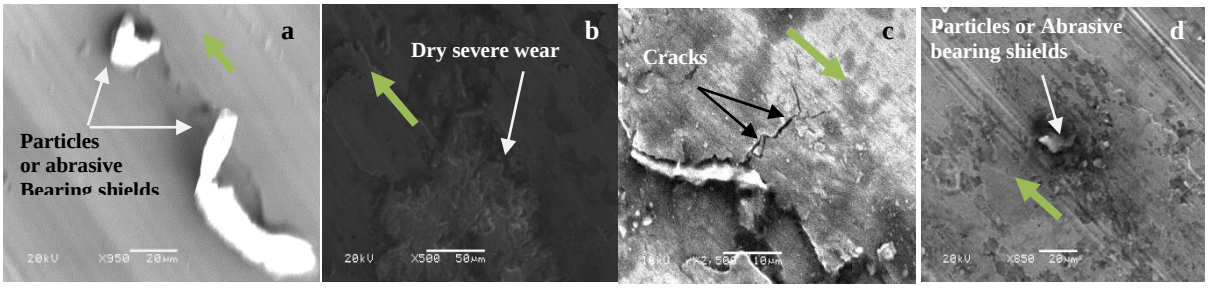

Figure 16. Images in (EDS, SEM), of the cylinder (a, b) and pin (c, d) tracks after test using (X500, X1000): (a, d) lubricated contact Ra_7 = 1.51[µm] and (b, c) dry contact Ra_3 = 0.98[µm]

The work of deformation of the asperities, in sliding, causes an increase of the friction force and the deformations generate the phenomenon of wear accompanied by a mutual metallic transfer between the facing surfaces (Figure 16, 17) [30, 31]. Indeed, during the test when surface wear occurs, the formation and agglomeration of the debris cause a profound change in contact (see Figure 16). The consequence of the latter is the reduction of the surface roughness as shown in Figure 16(a).

Figure 17, shows that energy dispersive spectroscopy (EDS) observations combined with scanning electron microscopy (SEM) data have detected the degradation characteristics in worn surfaces. The EDS spectrum associated with the particle shown in Figure 19(a), reveals the presence of manganese, which proves that these particles come from the material of the pins (transfer of material from the pin to the cylinder). It is suggested that this debris is the result of the micro-scaling and fragmentation of the low hardness pin material induced by the cumulative shear as suggested by Lepesant and Bouchoucha [32, 33].

For the hard pin under study, at an applied load of 20N, the worn surface of the track has micro-grooves and a smooth surface with plowing cracks (see Figure 16(a)). A test marks the presence of plastic deformations and tearing of materials (see Figure 17(b)). Moreover, micro-flaking and the resulting fine particles were observed on the micro-grooves generated asserting shear mechanisms, already indicated by Elhadi and Mouadji [30, 31]. The analysis by EDS confirmed that these particles consist mainly of oxidized material of the cylinder, because only very little chromium element has been detected.

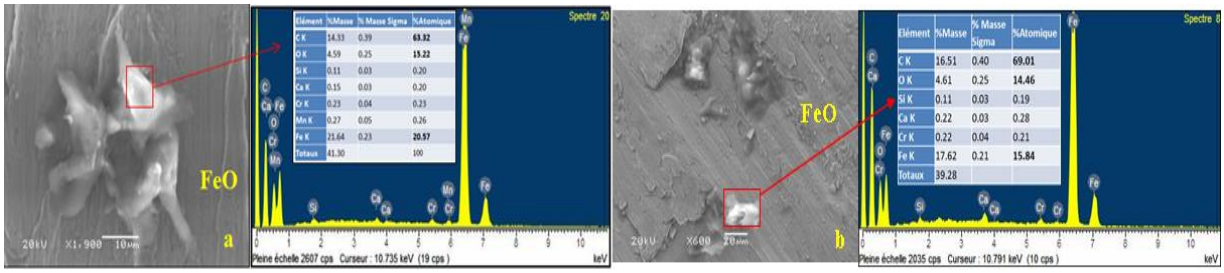

Figure 17. Image in (EDS) of the cylinder tracks specters and the pins after at 20 [Kv]: (a) Cylinder site lubricated contact, (b) Pin site lubricated contact

CONCLUSION

This study leads us to observe and substantiate several phenomena, namely:

- Roughness has a decreasing relation with cutting speed, has an inverse relation to the tool nose radius and a proportional one to the feed rate.
- The interaction between the different cutting parameters enabled good quality.

- Mathematical model has been developed. It is found that there is a significant coherence between the experimental and the values estimated.
- After tribology, a reduction in the maximum value of roughness Ra due to the disappearance of the peaks under the effect from higher shears stress at the level of the asperities. This phenomenon yields a considerable wear of the cylinder surface.
- During the dry contact, the roughness of the cylinder influences the wear rate W of the pin, resulting in the presence of three phases during friction coefficient variation.
- The presence of micro-cracks and particles on dry surfaces, which explains how easily material can be removed by abrasion due to the presence of a third body.
- On the worn cylinder surface, were presented micro-grooves, a smooth surface with cracks and plastic deformations. In addition, a material removal has been detected.
- During plastic deformation, oxidation process was noticed as the temperature increases.
- The lubricant has been employed to regulate the temperature, evacuate the abrasive grains, and minimize vibrations in order to allow the sliding of the surfaces in contact.

REFERENCES

[1] J. Cecha and al, "Surface roughness reduction using spray-coated hydro-gen silsesquioxane," *Appl. Surf. Sci.*, vol. 280, pp. 424– 430, 2013.

[2] A. Boryczkoand and al, "Effect of waviness and roughness components on trans-verse profiles of turned surfaces," *Measurement*, vol. 46, pp. 688–696, 2013.

[3] J.R. Guddat and al, "Hard turning of AISI 52100 using PCBN wiper geometry inserts and the resulting surface integrity," *1st (CIRP) Conference on Surface Integrity (CSI), Procedia Engin*, vol.19, pp.118–124, 2011.

[4] H. Aouici, M.A. Yallese, B. Fnides, K. Chaoui, T. Mabrouki, "Modeling and optimization of hard turning of X38CrMoV5-1 steel with CBN tool: Machining parameters effects on flank wear and surface roughness," *J. of Mech. Sci. and Tech*., vol. 25, no. 11, pp. 2843-2851, 2011.

[5] S. Sahua, B.B. Choudhury, "Optimization of surface roughness using Taguchi methodology & prediction of tool wear in hard turning tools," *Materials Today: Proceedings*. 2, pp. 2615 – 2623. 2015.

[6] S.V. Wagh, D.V. Bhatt, J.V. Menghani, S.S. Bhavikatti, "Effects of laser hardening process parameters on hardness depth of Ck45 steel using Taguchi's optimization technique," *IOP Conf. Series: Materials Science and Engineering*, vol. 810, 2020, doi: 10.1088/1757-899X/810/1/012027.

[7] J.V. Menghani, A. Govande, S.R. More, "Investigation on erosion wear behaviour of Cr2O3 plasma Thermal spray coating and Ni based hard facing by welding with Taguchi approach," *International Journal of Modern Manufacturing Technologies*, ISSN 2067–3604, vol. IX, no. 2 , 2017.

[8] J.F. Archard, "Contact and rubbing of flat surfaces," *Appl. Phys*, vol. 34, pp. 981-988, 1953.

[9] M. Kerridge, J .K. Lancaster, "The stages in a process of severe metallic wear," *Proc. Roy. Soc. Lond. A*, vol. 236, pp. 250–264, 1956.

[10] J. Ayel, "Les différentes formes tribologiques d'usure des surfaces métalliques," *Rev.*, vol. 31, no. 4, pp. 703-728, 1976.

[11] B. Bhushan, "Principle and Applications of Tribology," *New York: John Wiley & Sons*, In, 1999.

[12] J.D. Bressana, D.P. Darosa, A. Sokolowskib, R.A. Mesquitac & C.A. Barbosad, "Influence of hardness on the wear resistance of 17-4 PH stainless steel evaluated by the pin-on-disc testing," *J. of mat. Proc. Tech*. vol. 205, pp. 353-359, 2008.

[13] N. Khanafi-Benghalem, E. Felder, K. Loucif and P. Montmitonnet, "Plastic deformation of 25CrMo4 steel during wear: Effect of the temperature, the normal force, the sliding velocity and the structural state," *Wear*, vol. 268, pp. 23-40, 2010.

[14] C.C. Viáfara and A. Sinatora, "Influence of hardness of the harder body on wear regime transition in a sliding pair of steels," *Wear*, vol. 267, no. 1, pp. 425-432, 2009.

[15] V. Panin, A. Kolubaev, S. Tarasov and V. Popov, "Subsurface layer formation during sliding friction," *Wear*, vol. 249, pp. 860-867, 2002.

[16] N. Diomidis and S. Mischler, "Third body effects on friction and wear during fretting of steel contacts," *Trib. Intern*., vol. 44, no. 11, pp. 1452-1460, 2011.

[17] S.Q. Wang, M.X. Wei and Y.T. Zhao, "Effects of the tribo-oxide and matrix on dry sliding wear characteristics and mechanisms of a cast steel," *Wear*, vol. 269, no. 5, pp. 424-434, 2010.

[18] H. Bouhabila, A. Bouchoucha, R. Benzerga, C. Le Paven, "Surface quality effect on tribological behavior," *J. of New Tech. & Mat.*, vol. 08, no. 03, pp. 102-106, 2019.

[19] R. Suresh, "Some studies on hard turning of AISI 4340 steel using multilayer coated carbide tool," *Measurement*, vol. 45, pp. 1872–1884, 2012.

[20] M. Xiaoa, Q.M. Wanga, K. Satob, S. Karubeb, T. Soutomeb, H. Xua, "The effect of tool geometry on regenerative instability in ultrasonic vibration cutting," *Int. J. of Mach.Tools & Manuf*., vol.46, pp. 1–8, 2005.

[21] M. Sortino, "Dry turning of sintered molybdenum," *J. of Mat. Proc. Tech.*, vol. 213, pp. 1179 –1190, 2013.

[22] I. Meddour, M.A. Yallese, H. Bensouilah, A. Khellaf & M. Elbah, "Prediction of surface roughness and cutting forces using RSM, ANN, and NSGA-II in finish turning of AISI 4140 hardened steel with mixed ceramic tool," *The Int. J. of Adv. Manuf. Tech.*, vol. 97, pp. 1931–1949, 2018.

[23] L. Bidi, S. Mattei, E. Cicala, H. Andrzejewski, P. Le Masson, J. Schroeder, "The use of exploratory experimental designs combined with thermal numerical modelling to obtain a predictive tool for hybrid laser/MIG welding and coating processes," *Optics & Las. Tech.*, vol 43, no. 3, 4, pp. 537-545, 2011.

[24] S.R. More, D.V. Bhatt, J.V. Menghani, "Study of the parametric performance of solid particle erosion wear under the slurry pot test rig," *Tribology in Industry*, vol. 39, no. 4, pp. 471-481, 2017, doi:10.24874/ti.2017.39.04.06.

[25] A. Khellaf, H. Aouici, S. Smaiah, S. Boutabba, M.A. Yallese, M. Elbah, "Comparative assessment of two ceramic cutting tools on surface roughness in hard turning of AISI H11 steel: including 2D and 3D surface topography," *The Int. J. of Adv. Manuf. Tech.*, vol. 89, pp. 333–354, 2017.

[26] O. Zerti, M.A. Yallese, R. Khettabi, K. Chaoui, T. Mabrouki, "Design optimization for minimum technological parameters when dry turning of AISI D3 steel using Taguchi method," *The Int. J. of Adv. Manuf. Tech.*, vol. 89, pp. 915–1934, 2017.

[27] G. Kibria and al, "Experimental investigation and multi-objective optimization of Nd: YAGlaser micro-turning process of alumina ceramic using orthogonal array and grey relational analysis," *Opt. & Las. Tech.*, vol. 48, pp. 16–27, 2013.

[28] T. Leppert, "Effect of cooling and lubrication conditions on surface topo-graphy and turning process of C45 steel," *Int. J. of Mach.Tool. & Manuf.*, vol. 51, pp. 120–126, 2011.

[29] J. Wang and al, "Preparation and tribological properties of calcium perrhenate as high-performance lubricating additive toward a broad temperature range," *Jma. Terrs. Tech.*, vol. 9, no. 3, pp. 6579–6594, 2020.

[30] A. Elhadi, A. Bouchoucha, W. Jomaa, Y. Zedan, T. Schmitt, P. Bocher, "Study of surface wear and damage induced by dry sliding of tempered AISI 4140 steel against hardened AISI 1055 steel," *Trib. in Ind.*, vol. 38, no. 4, pp. 475-485, 2016.

[31] Y. Mouadji, M.A. Bradai, R. Younes, A. Sad-eddine, A. Benabbas, "Influence of heat treatment on microstructure and tribological properties of flame spraying Fe–Ni–Al alloy coating," *J. of C. South Univ.*, vol. 25, no. 3, 2018.

[32] P. Lepesant, C. Boher, Y. Berthier and F. Rezai-Aria, "A phenomenological model of the third body particles circulation in a high temperature contact," *Wear*, vol. 298-299, pp. 66-79, 2013.

[33] A. Bouchoucha, S. Chekroud, D. Paulmier, "Influence of oxygen on the tribological behavior on friction and wear in the couple copper-steel crossed by an electrical current," *Tribotest Journal*, vol. 11, no. 1, pp. 11-27, 2004.